

# SPECKLE IN OPTICAL COHERENCE TOMOGRAPHY

J. M. Schmitt, S. H. Xiang, and K. M. Yung

Hong Kong University of Science and Technology, Department of Electrical and Electronic Engineering, Clear Water Bay, Kowloon, Hong Kong

(Paper CDO-001 received Dec. 24, 1997; revised manuscript received Nov. 20, 1998; accepted for publication Nov. 24, 1998.)

## ABSTRACT

Speckle arises as a natural consequence of the limited spatial-frequency bandwidth of the interference signals measured in optical coherence tomography (OCT). In images of highly scattering biological tissues, speckle has a dual role as a source of noise and as a carrier of information about tissue microstructure. The first half of this paper provides an overview of the origin, statistical properties, and classification of speckle in OCT. The concepts of *signal-carrying* and *signal-degrading* speckle are defined in terms of the phase and amplitude disturbances of the sample beam. In the remaining half of the paper, four speckle-reduction methods—polarization diversity, spatial compounding, frequency compounding, and digital signal processing—are discussed and the potential effectiveness of each method is analyzed briefly with the aid of examples. Finally, remaining problems that merit further research are suggested. © 1999 Society of Photo-Optical Instrumentation Engineers. [S1083-3668(99)01401-X]

**Keywords** speckle; optical coherence tomography (OCT).

## 1 INTRODUCTION

The word “coherence” in optical coherence tomography (OCT)<sup>1–4</sup> conveys both a primary strength and a primary weakness of this new technology. On the one hand, the measurement technique on which OCT is based, interferometry, relies inherently on the spatial and temporal coherence of the optical waves backscattered from a tissue. On the other hand, this same coherence gives rise to speckle, an insidious form of noise that degrades the quality of OCT images. Speckle noise reduces contrast and makes boundaries between highly scattering structures in tissue difficult to resolve.

But is speckle actually a source of noise in OCT or is it the signal itself? After all, OCT can be classified as a special adaptation of electronic speckle pattern interferometry or holography<sup>5</sup> and one could argue (with some justification) that if all of the speckle in an image of dense tissue could somehow be removed entirely, no image would remain.

This paper gives an overview of speckle in optical coherence tomography and attempts to clarify some of the issues that make its origins and consequences difficult to understand. The basic properties of coherent noise in OCT images are addressed first and then various techniques for speckle reduction are outlined. The paper concludes with a short list of remaining problems for future research.

## 2 CHARACTERISTICS OF SPECKLE IN OCT

Speckle came to the forefront soon after it was discovered that the reflection of a laser beam from a rough surface has a distinctive granular or mottled appearance.<sup>6</sup> Having no obvious relationship with the texture of the surface, the dark and bright spots formed by the reflected beam change their pattern whenever the surface moves slightly. This phenomenon, known as laser speckle, was found by early researchers to result from random interference between reflected waves that are mutually coherent. It has taken several decades, however, for researchers to realize the full significance of speckle as a fundamental property of signals and images acquired by all types of narrowband detection systems, which include radar, ultrasound, and radio astronomy. In addition to the optical properties and motion of the target object, speckle is influenced by the size and temporal coherence of the light source, multiple scattering and phase aberrations of the propagating beam, and the aperture of the detector. All of these variables contribute to the observed characteristics of speckle in optical coherence tomography of living tissue. A thorough analysis of each of these variables alone and in combination is not possible within the narrow confines of a short overview paper. We ask the reader to settle instead for a barebones analysis of a small subset of these variables whose effects have been studied at this early stage of development of OCT. Many of the missing elements in the analysis presented in this section can

Address all correspondence to Joseph M. Schmitt. Tel: (852)2358-8515; Fax: (852)2358-148; E-mail: eeschmitt@ee.ust.hk

be pieced together from the theoretical analyses given in Ref. 7. Other elements are truly missing and an analysis of their influence on OCT awaits further research.

## 2.1 ORIGIN

In optical coherence tomography the sample is placed in one of the arms of an interferometer at the focus of a converging lens. As the optical path in the other arm of the interferometer varies during the scanning operation, an ac current is generated by a photodetector at the output of the interferometer. This photocurrent is proportional to the real part of the cross-correlation product of the reference optical field  $U_r$  and the optical field  $U_s$  backscattered from the sample,

$$i_d \sim \text{Re}\langle U_r U_s^* \rangle, \quad (1)$$

where the brackets  $\langle \rangle$  denote an average over time and space. When the light source satisfies the quasi-monochromatic condition (i.e., its center frequency  $\nu_0$  greatly exceeds its bandwidth  $\Delta\nu$ ) and the sample field backscatters from a single scattering center, the photocurrent can be expressed in terms of the optical path difference  $\tau$  between the two arms,

$$i_d(\tau) = K |g(\tau)| \cos[2\pi\nu_0\tau + \phi(\tau)], \quad (2)$$

where  $K$  is a constant of proportionality that relates the optical and electronic variables and  $|g(\tau)|$  and  $\phi(\tau)$  are, respectively, the argument and phase of the cross correlation in Eq. (1). The function  $|g(\tau)|$  describes the envelope of the temporal coherence function, given by  $g(\tau) = \langle U_s(t) U_s^*(t + \tau) \rangle$ . We see from Eq. (2) that  $i_d(\tau)$  responds to both the phase and the amplitude of the cross correlation of the scattered and reference optical fields. It is the sensitivity of the photocurrent to the phase that makes OCT susceptible to the effects of speckle. For the ideal case of a perfectly flat reflector placed at the focus of the lens in the sample arm, the complex autocorrelation function of the source determines the magnitude of the phase term  $\phi(\tau)$  in Eq. (2). However, when the sample is a tissue containing densely packed scatterers, both  $|g(\tau)|$  and  $\phi(\tau)$  can no longer be treated as deterministic variables because waves from multiple scattering centers combine randomly to form the interference signal.<sup>8</sup>

Consider the changes that a focused wave incident on the tissue undergoes as it propagates through the tissue to the sample volume, scatters back, and then propagates once again through the tissue back to the lens (Figure 1). Two main processes influence the spatial coherence of the returning wave: (1) multiple backscattering of the beam inside and outside of the desired sample volume and (2) random delays of the forward-propagating and returning beam caused by multiple forward scattering. Although the first of these is the primary

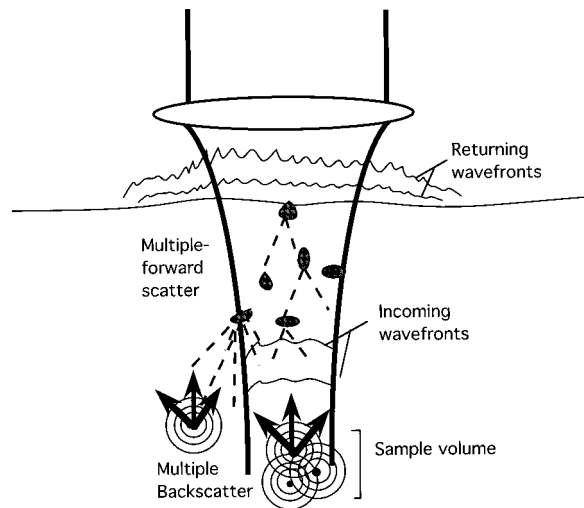


**Fig. 1** Propagation of a focused beam in tissue. The two main processes that distort the wave front of the returning wave—multiple forward scatter and multiple backscatter—are depicted here.

source of speckle in rough-surface imaging, the second must also be considered in coherent imaging systems like OCT, that utilize penetrating waves. The common feature of both processes is that they alter the shape of the wave front of the returning beam and create localized regions of constructive and destructive interference that appear as speckle in OCT images.<sup>9</sup> Multiple backscattering can occur in spite of the short coherence time of the sources used in OCT (usually less than 100 fs). For speckle to form, all that is required is that two or more scatterers in the sample volume backscatter waves that reach some point on the detector out of phase within an interval of time less than the coherence time of the source. Waves backscattered from any pair of point scatterers separated by an optical distance close to an odd multiple of one half of the wavelength can generate speckle, provided that the optical distance does not exceed the coherence length of the source in the medium. Waves backscattered from different facets of a single large particle can generate speckle in a similar manner. Recent studies suggest that closely packed subwavelength-diameter particles contribute a large fraction of the total optical cross section of tissue.<sup>10–12</sup> Therefore, the likelihood of finding a pair of scatterers or cluster of scatterers within the sample volume that satisfy the conditions for speckle generation is high.

The simulation results in Figure 2 illustrate how interference noise caused by multiple backscattering can distort the envelope of an OCT signal generated as the sample beam scans along a single line (an OCT “A line”). The coherent A line shown in Figure 2 was computed by convolving a random sequence of scatterers (top line of Figure 2) with the theoretical coherent point-spread function (PSF) of

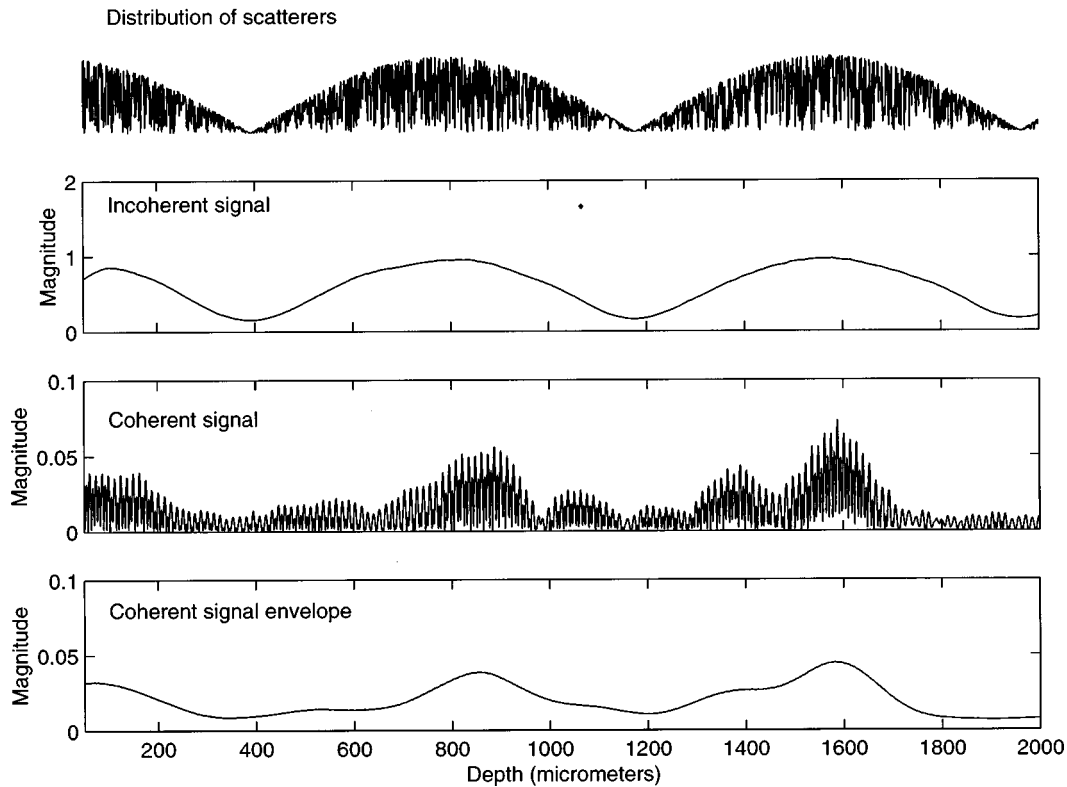


**Fig. 2** Simulation of the distortion of an OCT A line caused by the coherent detection process. The uppermost plot shows the ideal backscatter profile generated by a dense random distribution of point particles with cross sections modulated by a sinusoidal function. Below this plot is the incoherent signal that was formed by convolving the backscatter profile with the Gaussian envelope of the simulated OCT point-spread function ( $15 \mu\text{m}$  FWHM). The coherent signal was formed in a similar way by convolving the backscatter profile with the coherent PSF containing the optical carrier frequency. The lowermost plot is a low-pass filtered version of the coherent signal.

an OCT scanner; the incoherent A line was computed by convolution with the envelope of the PSF. Details of the simulation method are described in Ref. 13. Notice that, unlike those of the incoherent A line, the variations in the magnitude of the coherent A line track the density of scatterers poorly. In two-dimensional OCT images formed from a series of A lines, this type of distortion manifests itself as speckle.

## 2.2 STATISTICAL PROPERTIES

Figure 3 is an example of an OCT image that shows high-contrast speckle in regions of strong backscatter below the surface of skin. Notice that the appearance of the speckle noise has no obvious dependence on depth, which suggests that the statistical properties of the speckle are dominated by the effects of multiple backscatter, rather than by phase aberrations incurred during propagation through overlying tissue. Decorrelation of the incident and returning beams undoubtedly also occurs, but its effects are difficult to discern because the phase aberrations caused by the multiple forward scattering and multiple backscattering processes superimpose. When a large number of polarized quasimonochromatic waves with random phase

combine, a fully developed speckle pattern is formed in which the probability of measuring an intensity  $I$  at a given point is described by the negative-exponential density function,<sup>14</sup>

$$p(I) = \frac{1}{\langle I \rangle} \exp\left[-\frac{I}{\langle I \rangle}\right], \quad (3)$$

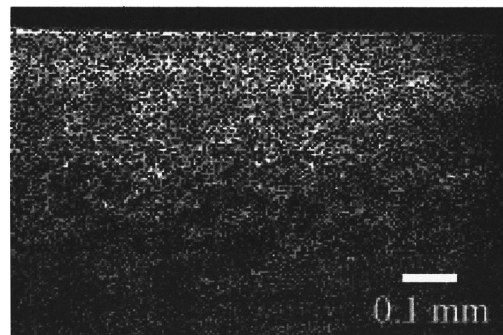


**Fig. 3** Example of an OCT image (dorsal aspect of a finger) containing high-contrast speckle. The interference signals from which the image was formed were sampled at  $1.2 \mu\text{m}$  intervals in both dimensions and the overall size of the image is approximately  $1 \text{ mm} \times 1 \text{ mm}$ .

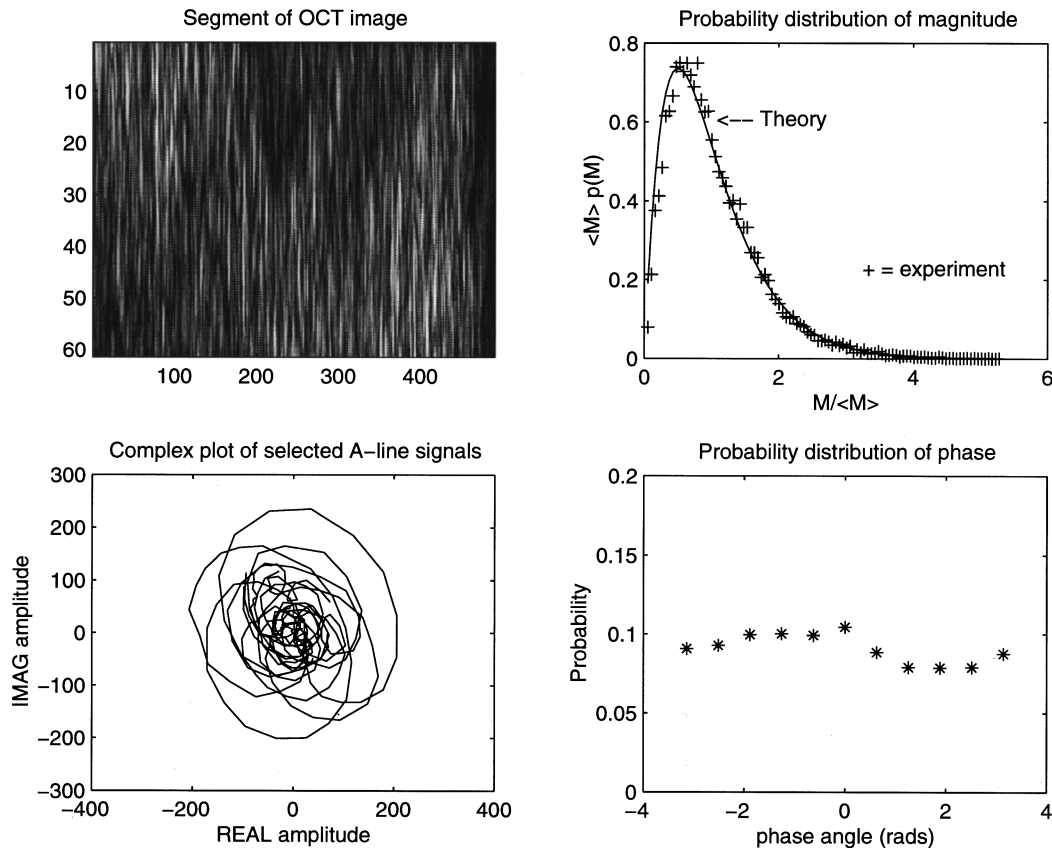


**Fig. 4** Statistics of the amplitude and phase variations of the OCT interference signal derived from a highly scattering region of living skin tissue. Upper left: OCT image of the region of the tissue from which the signals were extracted. Upper right: Histogram of the signal magnitude  $M = \sqrt{A_s^2 + A_c^2}$ , where  $A_s$  and  $A_c$  are the amplitudes of the real (cosine) and imaginary (sine) components of the quadrature demodulated interference signal. The measured data are fit by the solid-line curve which is a plot of Eq. (4). Lower right: Histogram of the measured phase, defined as  $\tan^{-1}(A_s/A_i)$ . Lower left: Plot of the real and imaginary components of three A line signals plotted together in the complex plane.

where  $\langle I \rangle$  is the mean intensity. The image of a speckle pattern that obeys negative-exponential statistics has a signal-to-noise ratio (SNR) equal to 1, where the SNR is defined as the ratio of the mean and standard deviation of the intensity,  $SNR = \langle I \rangle / \sigma_I$ . Because intensities close to zero are probable, fully developed speckle patterns are riddled with dark spots.

Although the ac photocurrent  $i_d$  measured by OCT scanners is proportional to the complex cross correlation  $\langle U_r U_s^* \rangle$ , not the intensity  $I = \langle U_s U_s^* \rangle = \langle |U_s|^2 \rangle$  in Eq. (3), its squared magnitude  $M = i_d^2$  can nevertheless be treated as an analog of the intensity for characterization of the statistical properties of speckle in OCT images. To study these properties, we employed a quadrature-demodulation technique to record the instantaneous phase and amplitude of the ac photocurrent from an OCT scanner.<sup>15</sup> Figure 4 presents the results of a typical set of measurements. Histograms of the intensities and phases of the OCT signals acquired from a highly scattering region of the skin are shown in the right half of Figure 4. As expected from the random nature of the signals, the phase was found to be

almost uniformly distributed between  $-\pi$  and  $\pi$  (Figure 4, lower right). The lack of correlation between the real and imaginary components of complex amplitudes of the measured OCT signals gives further evidence of the randomness of the phase. Plotted as a curve in the complex plane, the trajectory of the complex amplitude of the signals recorded along a given A line was found to execute a random walk within a circular area centered on the origin (Figure 4, lower left). We found a close fit between the histograms of  $M$  and the density function expected for speckle generated by reflection of unpolarized light from a rough surface,

$$p(M) = \frac{4M}{\langle M \rangle^2} \exp \left[ -2 \frac{M}{\langle M \rangle} \right]. \quad (4)$$

A close relative of the Rayleigh distribution, this density function describes the random variations in the sum of two oppositely polarized intensities in a speckle field, each of which obeys negative-exponential statistics.<sup>16</sup> The SNR of the unpolarized intensity in an unpolarized speckle field is 1.4, a value higher than that of the negative-exponential

density function (SNR=1), but lower than that of the Rayleigh density function (SNR=1.9). Insofar as the open-air interferometer with which the measurements were made is designed to respond equally well to light backscattered in either polarization state, the theoretical conditions underlying the derivation of Eq. (4) are consistent with the experimental conditions. However, it would be presumptuous to claim that Eq. (4) is a universal description of the first-order statistics of the OCT signal magnitude, because the effects of the bandwidth of the source, the aperture of the collection optics, and other instrumental variables are not yet known. Previous studies in other fields indicate, however, that these variables do not alter the first-order statistics of the speckle, except when the number of scatterers in the sample volume is small or the distribution of scatterers is periodic.<sup>17</sup> Preliminary measurements suggest that the SNRs of OCT images of biological tissue lie between 0.5 and 2.0,<sup>3,15,18,19</sup> a range that encompasses the SNRs of polarized and unpolarized speckle patterns.

### 2.3 CLASSIFICATION

The results of the experiments and simulations discussed thus far underscore the importance of multiple backscatter in the formation of speckle in OCT. This type of speckle can be classified as noise because it reduces the correspondence between the local density of scatterers and the intensity variations in OCT images. If somehow all of waves backscattered from the sample volume could be forced to interfere constructively, the noise would vanish and the contrast of features in the OCT image would be markedly improved. The speckle-reduction techniques discussed in the next section (Sec. 3) aim toward this ideal.

A fundamental problem arises, however, when the objective of removing speckle is extended to the extreme of removing speckle entirely. It is here that the types of speckle that we call *signal-carrying* speckle and *signal-degrading* speckle need to be introduced.

The richest source of information in optical coherence tomography is the single-backscattered component of the scattered optical field, because its spatial-frequency content extends to the diffraction limit of the imaging optics. Unfortunately, for single backscattering to occur, the incident beam must pass through the overlying tissue without scattering, reflect from one (and only one) particle in the focal plane, and then return to the detector, again without scattering within the overlying tissue. When an optically dense tissue is probed, the probability that only this type of scattering occurs within the temporal coherence interval is diminishingly small. In practice, the returning optical field is corrupted by speckles with correlation spot sizes ranging from less than a wavelength (generated by near-simultaneous backscattering from widely

separated particles illuminated by multiply scattered light) to several hundred micrometers (generated by narrow-angle forward scattering and multiple backscattering by large particles) to more than the diameter of the lens (generated by the single-backscattered light). In OCT, the signal-carrying speckle originates from the sample volume in the focal zone of the imaging optics and projects the largest average spot size. The signal-degrading speckle field consists of small speckle spots created by the out-of-focus light that scatters multiple times and happens to return within the delay time set by the difference between the optical paths in the two arms of the interferometer. Fortunately, the ability to discriminate between signal-carrying and signal-degrading speckle is an inherent characteristic of a scanning interferometer that can be controlled to some extent by the numerical aperture (NA) of the imaging optics. The component of the optical field corrupted by many small speckle spots generates, on average, an interference signal of nearly zero amplitude that fluctuates little as the optical path difference between the arms of the interferometer is scanned. For this reason, the speckle produced by wide-angle multiply scattered light is relatively easy to suppress in OCT. The rms amplitude of the fluctuations produced during scanning by the large speckles in the field is comparatively high. Unfortunately, because of the unfavorable nature of the statistical properties of speckle, a few large speckles or many small speckles are almost equally likely to produce signal amplitudes close to zero for a given sample of the speckle field and only the second-order statistics (i.e., spatial distribution) of the signal-carrying and signal-degrading speckle differ significantly.

The question posed in the introduction regarding whether speckle is the signal or the noise in OCT can now be answered succinctly: it is both. To differentiate signal from noise, a well-designed scanner accentuates the interference signals generated by the component of the measured optical field that contains the largest speckles and suppresses the others.

### 2.4 THE MISSING FREQUENCY PROBLEM

The earlier subsections discuss speckle from the classical perspective as an interference phenomenon. There is an equivalent, yet much broader, interpretation of speckle to which Fercher et al.<sup>20</sup> and Hellmuth<sup>21</sup> alluded in earlier papers that has important implications for OCT imaging. This interpretation relates to the missing frequency problem,<sup>22</sup> which is best understood in the context of information processing. Suppose that we regard the desired signal in OCT as a three-dimensional distribution of refractive-index variations characterized by a certain spatial-frequency spectrum  $S(\nu)$ , as illustrated in Figure 5.  $S(\nu)$  extends from  $1/R_0$  to  $1/r_0$ , where  $R_0$  is the dimension of the largest con-

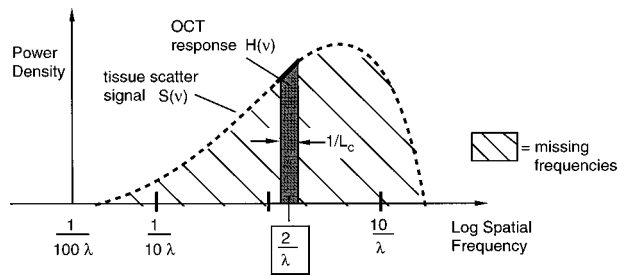


**Fig. 5** Illustration of the disparity between the broad spatial-frequency spectrum of the refractive index variations in tissue  $S(\nu)$  and the narrow spatial-frequency response of an OCT scanner  $H(\nu)$ . Given by the magnitude of the Fourier transform of the coherent point-spread function,  $H(\nu)$  is centered on the peak wavelength of emission of the source  $\lambda$  and has a width equal to the reciprocal of the coherence length  $l_c$ .

tinuous structure in a given volume of tissue (e.g., a blood vessel) that gives a measurable backscatter signal and  $r_0$  is the smallest (e.g., a protein macromolecule). Owing to the nature of the coherent detection method on which it is based, OCT scanners can detect only those objects whose spatial-frequency spectra overlap the band of spatial frequencies between  $[2/\lambda - 1/l_c, 2/\lambda + 1/l_c]$ , where  $l_c$  is the coherence length of the source.<sup>21</sup> A consequence of this bandpass characteristic is that the

interior of structures with smoothly varying refractive-index profiles are absent in OCT images. Figure 6 illustrates this effect. The simulated OCT image in the upper right of Figure 6 was made by convolving the image of a stained tissue section of skin (upper left of Figure 6) with the theoretical coherent PSF of an OCT scanner ( $l_c = 15 \mu\text{m}$ ; lateral focal-spot diameter =  $10 \mu\text{m}$ ) given in Ref. 13. Notice the severe distortion of the simulated OCT, in comparison with the incoherent image which was computed by convolving the image of the tissue section with the envelope of the PSF (lower left of Figure 6). The power-spectral density curves in the lower right of Figure 6 show the distortion of the spatial-frequency spectrum of the original image caused by the bandpass filtering property of the coherent detection process. Interestingly, in this example the loss of low spatial frequencies appears to have degraded the image quality most. Although blurred noticeably by the attenuation of high spatial frequencies above  $1/l_c = 67 \text{ mm}^{-1}$ , the incoherent image in this example retains most of the structural detail of the unprocessed tissue section.

This example demonstrates that OCT images suffer from a type of speckle whose effects can be appreciated without directly invoking the concepts of random interference and multiple scattering. By

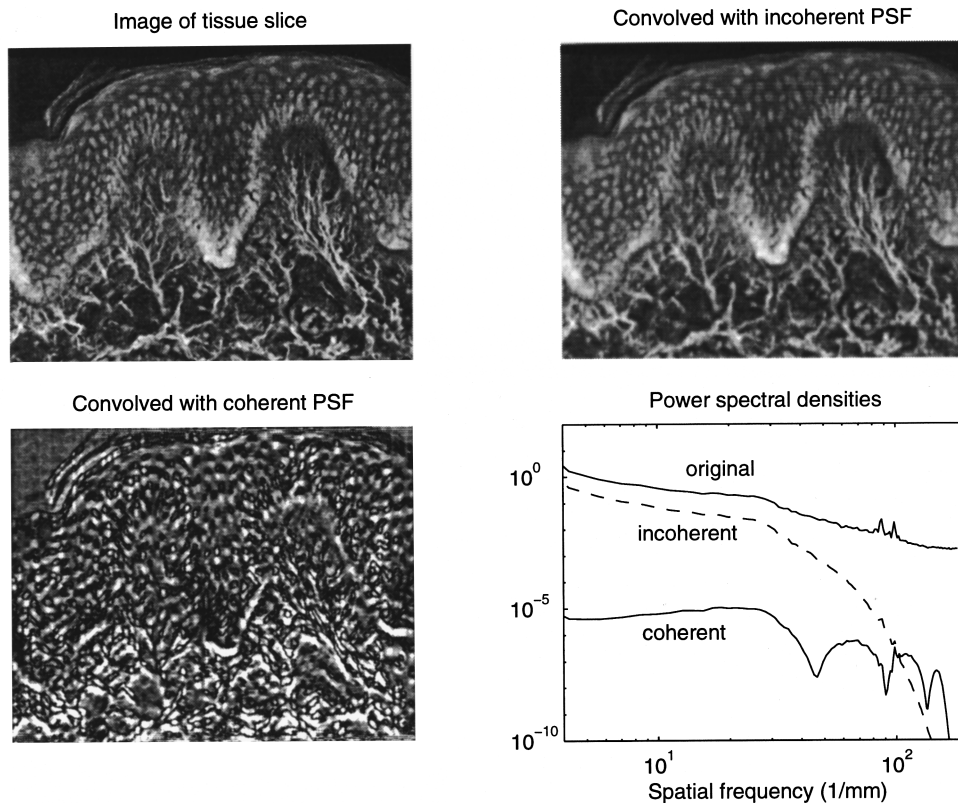


**Fig. 6** Simulation of the effect of the bandpass filtering property of the coherent detection process in OCT on image quality. Upper left: image of a stained tissue section of skin (approximately  $1 \text{ mm} \times 1 \text{ mm}$ ). Upper right: image after convolution with the envelope of the simulated point-spread function (PSF) of an OCT scanner. Lower right: image after convolution with the simulated coherent PSF of an OCT scanner. Lower right: one-dimensional power-spectral densities of the three images.

calling this type of noise "speckle," we risk stretching the definition of an already overstretched term. It would perhaps be better to classify this manifestation of speckle and classical speckle together simply as narrowband noise to emphasize their common origin. In fact, the simulation results in Figure 6 do not accurately represent scattering from real tissue, which contains particles much smaller than the pixels in the original image of the tissue section. Because such particles exist in abundance, truly continuous structures that extend over more than a few micrometers are rare; instead, large structures in tissue are assembled from smaller structures, each of which contributes to the total backscatter cross section. For this reason, the edge enhancement that results from the bandpass property of the coherent-detection process is not as apparent in OCT images of dense tissue. The small particles, in effect, outline the boundaries of the larger structures; as a result, the high- and low-frequency components of the spatial frequency spectrum of tissue tend to correlate.<sup>10</sup> This fortuitous situation makes OCT images look better than one would expect given the limitations of the coherent detection process.

### 3 SPECKLE REDUCTION

In the context of optical coherence tomography, the objective of speckle reduction is to suppress signal-degrading speckle and accentuate signal-carrying speckle. According to the definitions in Sec. 2.3, these two types of speckle are distinguished by their correlation spot sizes and by the frequencies of the signals they generate during scanning.

Speckle-reduction techniques fall into four main categories: polarization diversity, spatial compounding, frequency compounding, and digital signal processing. This section examines the applicability of each of these techniques to OCT imaging and outlines the results of the few studies that have been carried out to date. As the undiminished zeal of researchers toward the development of new speckle-reduction methods for medical ultrasound, astronomy, and other fields attests, none of these techniques has proved to be entirely satisfactory. One should not expect, therefore, that a ready solution exists for the speckle problem in OCT. Nonetheless, substantial improvement in image quality should be achievable through the skillful adaptation of available techniques. The preliminary results highlighted later in this section give evidence of the effectiveness of this approach.

#### 3.1 POLARIZATION DIVERSITY

Polarization diversity in OCT can be achieved simply by illuminating the sample with unpolarized light and interfering the backscattered light with an unpolarized reference beam. Most OCT scanners based on interferometers built with non-polarization-preserving single-mode fibers auto-

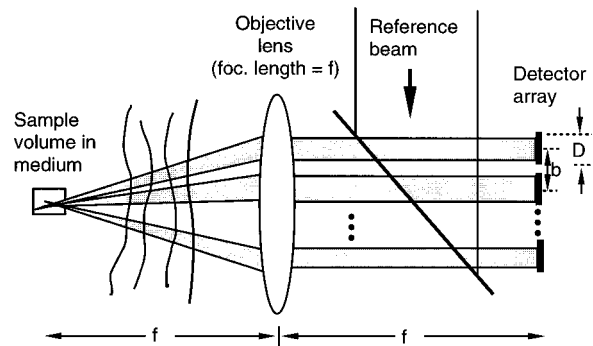


Fig. 7 Principle of angle compounding (from Ref. 15).

matically implement a form of polarization diversity. However, because most fiber-optic couplers are not completely polarization independent, equal mixing of light in opposite polarization states cannot be assumed. Configurations of polarization-independent interferometers have been reported for fiber-optic reflectometry which should work equally well for optical coherence tomography of biological tissue.<sup>23</sup> A limitation of polarization diversity is that it increases the SNR of a fully developed speckle pattern by a factor of  $\sqrt{2}$  at most. The actual increase in SNR that can be realized in OCT may be considerably less, however, because the polarization signal-carrying component of the speckle may maintain its polarization better than the signal-degrading component generated by multiple wide-angle scattering.

#### 3.2 SPATIAL COMPOUNDING

In spatial compounding, the absolute magnitudes of signals derived from the same sample volume or slightly displaced sample volumes are averaged to form a new signal with reduced speckle noise. It is essential that the signals add on a magnitude basis because addition of the amplitudes of signals derived from the different speckle patterns does not improve the SNR.<sup>14</sup> The effectiveness of this approach depends on the number of signals averaged and their mutual coherence. The incoherent average of  $N$  uncorrelated signals, each with the same signal-to-noise ratio  $\text{SNR} = S_R$ , yields a combined signal with a SNR equal to  $S_R \sqrt{N}$ . Any correlation among the signals reduces the SNR gain. Because the total field of view or angular aperture of the detector must be split to perform the averaging, spatial compounding always results in some loss of resolution.

Figure 7 illustrates one realization of spatial compounding, called angular compounding, that has been applied recently to OCT.<sup>19</sup> An array of detectors located in the back Fourier plane of the objective lens receives light backscattered from the sample volume at different angles. The absolute magnitudes of the demodulated photocurrents from each of the detectors are added to obtain a

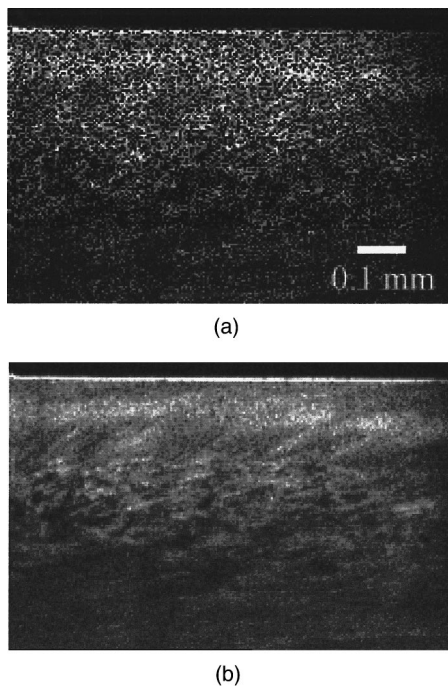


**Fig. 8** OCT images before and after angle compounding. The uncompounded image in (a) is the same as the image shown in Figure 3 and is repeated here for ease of comparison. It was formed from the magnitude of the signal measured by one element of a quadrant detector located in the back focal plane of the objective lens. To form the compounded image in (b), the square root of the sum of the squares of the interference signals from all four detectors was calculated for each pixel.

combined signal with reduced speckle variance. An advantage of this approach is that the number of detectors can be tailored for optimal separation of the signal-carrying speckle from the signal-degrading speckle. For best performance, the NA of the lens should be made as large as possible to increase the light collection angle of each detector, while still providing the working distance needed to achieve the desired probing depth.

OCT images of living skin acquired with and without angular compounding are compared in Figure 8. The uncompounded image was formed from the magnitude of the signal from a single detector in a quadrant array and the compounded image was formed from the sum of the signals from all four detectors. The increase in the number of discernible grayscale levels of the compounded image is a consequence of the enlarged numerical aperture of the combined detector and the reduced speckle contrast (increased SNR) of the averaged signal.<sup>19</sup> Assuming that the array fills the entire back focal plane of the lens, the extent to which the SNR can be improved at a given resolution using angular compounding is limited by the NA of the lens. As the NA increases, however, the spherical aberration caused by the refractive-index mismatch at the surface of the tissue becomes increasingly severe. At the same time, the sensitivity of the inter-

ference signal to phase and amplitude aberrations caused by dispersion of the sample beam within inhomogeneous tissue overlying the sample also increases. Unless corrected adaptively, these aberrations can reduce the resolving power to the extent that further increases in the NA above a certain limiting value would be fruitless. The numerical aperture above which aberrations dominate at a given probing depth depends on the optical properties of the tissue and other variables whose effects are still unknown.

Spatial compounding can be done with a single detector by scanning the reference beam back and forth across the detector plane within an interval much shorter than the time constant of the demodulator. This approach has been demonstrated in lidar using an acousto-optical technique,<sup>24</sup> but its application in OCT is complicated by the wide bandwidth of the light source which necessitates correction for optical dispersion in the acousto-optical scanner. A simple and inexpensive spatial-compounding technique for fiber-optic OCT imaging systems has not yet been reported.

### 3.3 FREQUENCY COMPOUNDING

Frequency compounding takes advantage of the reduced correlation between speckled images recorded within different optical frequency bands. To ensure sufficient decorrelation for effective averaging of the images, the overlap of the bands should be as small as possible. Suppose, for example, that the bandwidth  $\Delta\lambda$  of the light source of an OCT scanner with a peak emission wavelength of  $\lambda = 1.3\ \mu\text{m}$  is split into  $N$  equal, nonoverlapping bands. Since the phases of the fully developed speckle recorded with nonoverlapping sources are uncorrelated, incoherent addition of the images would reduce the speckle contrast by a factor of  $\sqrt{N}$ . However, the axial resolution, which is determined by the temporal coherence length of the source, would degrade at the same time by a factor of  $N$ . In OCT, this loss of resolution is a steep price to pay. A typical superluminescent diode with a peak emission wavelength of  $\lambda = 1.3\ \mu\text{m}$  and a full width at half maximum (FWHM) bandwidth of 30 nm has a coherence length in tissue (assuming a mean refractive index of 1.38) of approximately 18  $\mu\text{m}$ . Therefore, applying nonoverlapping frequency compounding to halve the speckle contrast with a typical source would degrade the axial resolution from 18  $\mu\text{m}$  to approximately 72  $\mu\text{m}$ . For most biomedical applications of OCT, such poor axial resolution would be unacceptable.

Melton and Magnin showed that the cross-correlation coefficient between fully developed speckle patterns formed in two equal-width Gaussian frequency bands with center frequencies separated by  $f_s$  is approximately<sup>25</sup>

$$\rho_{xy} = \exp\left[-\frac{f_s^2}{2B^2}\right], \quad (5)$$

where  $B$  is the width of each band. This correlation coefficient can be written equivalently in terms of the FWHM width of the emission spectrum of the source in wavelength units  $\Delta\lambda$  and the wavelength difference  $\lambda_s$  as

$$\rho_{xy} = \exp\left[-\frac{\lambda_s^2}{2\Delta\lambda^2}\right]. \quad (6)$$

According to Eq. (6), the cross-correlation coefficient remains high even for relatively large wavelength differences. For example, for  $\lambda_s = \Delta\lambda/2$ , which corresponds to an overlap between the bands of about 50%,  $\rho_{xy} = 0.88$ . But in OCT, the phase and amplitude aberrations of the sample beam that occur in the layers overlying the sample volume may cause more rapid decorrelation of the speckle with wavelength than Eq. (6) predicts. The wavelength dependence of the correlation depends on the mean scatter angle and the number of scattering events—the same factors that affect the speckle spot size. Thus, frequency compounding may provide a means of distinguishing the signal-carrying and signal-degrading speckle defined in Sec. 2.3. Reduction of speckle noise could be done adaptively by varying the compounding bandwidths according to the second-order statistics of the recorded image.

The preceding discussion points to the conclusion that a wideband source is a prerequisite for effective application of frequency compounding in OCT. A simple way to synthesize a source with a wider spectrum is to combine multiple light-emitting diode (LED) sources.<sup>26</sup> Unfortunately, LED sources generally emit less than 100  $\mu\text{W}$  in a single spatial mode and sources with peak emission wavelengths that differ by a few tens of nanometers are not readily available. If these problems can be solved, source synthesis may permit suppression of speckle by frequency compounding without unacceptable loss of resolution. Widening the source bandwidth has the additional benefit of filling in some of the missing spatial frequencies in the tissue spectrum lost in the coherent detection process (see Sec. 2.4).

### 3.4 DIGITAL SIGNAL PROCESSING

Numerous methods have been developed—and continue to be developed—for reducing speckle noise in coherent imaging systems. Most are applied after an image is formed and are commonly referred to as image postprocessing methods. The remaining methods are applied directly to the complex interference signal before the image is recorded and are referred to in this section as complex-domain processing methods.

Among the most popular image postprocessing methods for speckle reduction are median

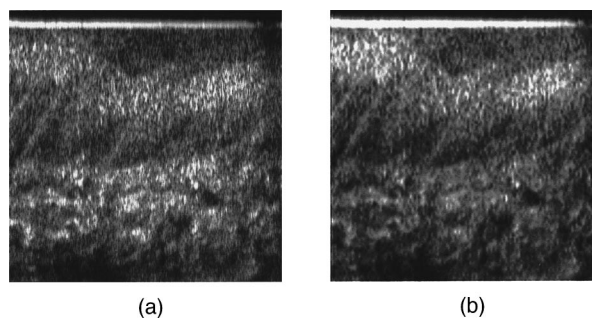


**Fig. 9** OCT images of living skin (a) before and (b) after wavelet processing for speckle reduction. Each image covers an area of approximately 0.5 mm (deep)  $\times$  1 mm (wide).

filtering,<sup>27</sup> homomorphic Weiner filtering,<sup>28</sup> multi-resolution wavelet analysis,<sup>18,29</sup> and adaptive smoothing.<sup>30</sup> All of these methods incorporate either an explicit or implicit statistical model of the spatial-frequency spectra of the target features and background. In the years since the demonstration of the first OCT scanners, the only image postprocessing method that has been reported specifically for speckle reduction in OCT is a wavelet filter that employs nonlinear thresholds.<sup>19</sup> The reported results indicate that when the frequency bands and thresholds are chosen properly wavelet filtering can improve the contrast-to-noise ratio of highly scattering features corrupted with speckle. The optimum shape of the passband of a conventional frequency-domain or wavelet-based filter can be derived from the ensemble-averaged spatial-frequency spectra of a group of histological tissue specimens with the same microstructure as the tissue being probed. However, insofar as the power-spectral densities of signal-carrying and signal-degrading speckle overlap, some loss of useful information is inevitable. By adjusting the passband according to the local mean or standard deviation measured within a window centered on the region of interest, the blurring across the boundaries of heavily speckled regions that results from loss of high-frequency information can be reduced.

Figure 9 illustrates the ability of the nonlinear wavelet filter described in Ref. 19 to suppress speckle noise at high spatial frequencies without blurring small features. Wavelet processing is useful for removing the fine granular noise that pervades OCT images of dense tissue. A comparison of Figures 9(a) and 9(b) shows the improvement in contrast that can be achieved by removing this type of noise.

A potential advantage of processing OCT interference signals in the complex domain is that changes in the phase as well as the amplitude of the signals can be used to distinguish signal-carrying from single-degrading speckle. One type of speckle-reduction method that operates in the complex domain, called the zero-amplitude procedure (ZAP), was first applied by Healey et al.<sup>31</sup> in medi-

cal ultrasound. It has been applied recently to optical coherence tomography by Yung et al.<sup>15</sup> ZAP relies on the location of the zeros of the interference signal in the complex plane to find gaps in the signal caused by destructive interference. After the zeros are located, their positions are rotated to fill in the gaps. Applied to OCT, this procedure appears to be quite effective in reducing speckle contrast, but tends to blur boundaries of features.<sup>15</sup>

Digital signal processing in the complex domain can also be used to implement a form of adaptive frequency compounding, as suggested in Sec. 3.3. Other complex-domain processing methods that have been applied in OCT include iterative point deconvolution (CLEAN<sup>32,33</sup>) and constrained iterative deconvolution.<sup>34</sup> Although not speckle-reduction methods *per se*, they share a similar aim of reducing the degrading effects of the sidelobes of the coherent PSF. Deconvolution of OCT signals performs best, in general, when the scattering targets are separated by the width of the envelope of the PSF or more; as the number of scatterers in the sample volume increases, the deconvolution becomes increasingly sensitive to noise and performance degrades steeply. This failure is related to the difficulty of interpolating between the gaps in the spatial-frequency spectrum that arise from the coherent detection process.<sup>22</sup>

#### 4 REMAINING PROBLEMS

Any overview of a topic as complex as speckle in OCT inevitably unearths a number of problems for future research. The following is a short list of problems that deserve special attention.

- Current understanding of the classes of speckle and their origins is sketchy. More experimental work is needed to explain the relationship between the microscopic scattering properties of tissue and the statistical properties of speckle in OCT images, particularly the second-order properties that specify the distribution of the correlation spot sizes in the projected speckle patterns.

- As a fundamental manifestation of coherent noise, speckle is a natural consequence of the limited spatial-frequency bandwidth of an interferometric measurement system. To enable effective suppression of speckle effects in OCT, techniques for simultaneously widening the bandwidth of the light source and the light collection aperture must be developed.

- Too few studies have focused on ways of adapting spatial- and frequency-compounding methods employed in synthetic-aperture radar and medical ultrasound to optical coherence tomography. More work in this area is needed.

- The applications of complex-domain processing in OCT merit further investigation, especially those techniques that exploit the phase of the OCT signal.

#### REFERENCES

1. D. Huang, E. A. Swanson, C. P. Lin, J. S. Schuman, W. G. Stinson, W. Chang, M. R. Hee, T. Flotte, K. Gregory, C. A. Puliafito, and J. G. Fujimoto, "Optical coherence tomography," *Science* **254**, 1178–1181 (1991).
2. C. K. Hitzenberger, W. Drexler, and A. F. Fercher, "Measurement of corneal thickness by laser doppler interferometry," *Invest. Ophthalmol. Visual Sci.* **33**, 98–103 (1992).
3. J. M. Schmitt, A. Knüttel, M. Yadlowsky, and R. F. Bonner, "Optical-coherence tomography of a dense tissue: Statistics of attenuation and backscattering," *Phys. Med. Biol.* **42**, 1427–1439 (1994).
4. J. A. Izatt, M. D. Kulkarni, H. W. Wang, K. Kobayashi, and M. V. Sivak, "Optical coherence tomography and microscopy in gastrointestinal tissues," *IEEE J. Sel. Top. Quantum Electron.* **2**, 1017–1028 (1997).
5. E. Leith, H. Chen, Y. Chen, D. Dilworth, L. Lopez, R. Masri, J. Rudd, and J. Valdmnis, "Electronic holography and speckle methods for imaging through tissue using femtosecond gated pulses," *Appl. Opt.* **30**, 4204–4210 (1991).
6. J. D. Rigden and E. I. Gordon, "Granularity of scattered optical maser light," *Proc. IRE* **50**, 6564–6574 (1962).
7. *Laser Speckle and Related Phenomena*, J. C. Dainty, Ed., Springer-Verlag, New York (1984).
8. L. Mandel and E. Wolf, *Optical Coherence and Quantum Optics*, pp. 401–414, Cambridge University Press, Cambridge (1995).
9. A. Wax and J. E. Thomas, "Measurement of smoothed Wigner phase-space distributions for small-angle scattering in a turbid medium," *J. Opt. Soc. Am. A* **15**, 1986–1908 (1998).
10. J. M. Schmitt and G. Kumar, "Turbulent nature of refractive-index variations in biological tissue," *Opt. Lett.* **21**, 1310–1312 (1996).
11. A. Dunn and R. Richards-Kortum, "Three-dimensional computation of light scattering from cells," *IEEE J. Sel. Top. Quantum Electron.* **2**, 898–905 (1996).
12. J. Beuthan, O. Minet, J. Helfmann, M. Herrig, and G. Müller, "The spatial variation of the refractive index in biological cells," *Phys. Med. Biol.* **41**, 369–382 (1996).
13. J. M. Schmitt and L. Zhou, "Deconvolution and enhancement of optical coherence tomograms," *Proc. SPIE* **2981**, 46–57 (1997).
14. J. W. Goodman, "Some fundamental properties of speckle," *J. Opt. Soc. Am.* **66**, 1145–1150 (1976).
15. K. M. Yung, S. L. Lee, and J. M. Schmitt, "Phase-domain processing of optical coherence tomography images," *J. Biomed. Opt.* **4**, 125–136 (1999).
16. J. W. Goodman, *Statistical Optics*, pp. 124–127, Wiley, New York (1985).
17. R. F. Wagner, M. F. Insana, and D. G. Brown, "Statistical properties of radio-frequency and envelope-detected signals with applications to ultrasound," *J. Opt. Soc. Am. A* **4**, 910–921 (1987).
18. J. M. Schmitt, "Array detection for speckle reduction in optical coherence microscopy," *Phys. Med. Biol.* **42**, 1427–1439 (1997).
19. S. H. Xiang, L. Zhou, and J. M. Schmitt, "Speckle noise reduction for optical coherence tomography," *Proc. SPIE* **3196**, 79–88 (1997).
20. A. F. Fercher, W. Drexler, and C. K. Hitzenberger, "Ocular partial coherence tomography," *Proc. SPIE* **2732**, 229–241 (1996).
21. T. Hellmuth, "Contrast and resolution in optical coherence tomography," *Proc. SPIE* **2926**, 228–237 (1997).
22. D. L. Fried, "Analysis of the CLEAN algorithm and implications for superresolution," *J. Opt. Soc. Am. A* **12**, 853–860 (1995).
23. M. Kobayashi, H. Hanafusa, K. Takada, and J. Noda, "Polarization-independent interferometric optical-time-domain reflectometer," *J. Lightwave Technol.* **9**, 623–628 (1991).
24. C. E. M. Strauss, "Synthetic-array heterodyne detection: A single-element detector acts as an array," *Opt. Lett.* **19**, 1609–1611 (1994).
25. H. E. Melton and P. A. Magnin, "A-mode speckle reduction

- with compound frequencies and compound bandwidths," *Ultrason. Imaging* **6**, 203–207 (1984).
26. J. M. Schmitt, S. L. Lee, and K. M. Yung, "An optical coherence microscope with enhanced resolving power," *Opt. Commun.* **142**, 203–207 (1997).
  27. R. Bernstein, "Adaptive nonlinear filters for simultaneous removal of different kinds of noise in images," *IEEE Trans. Circuits Syst.* **34**, 1275–1291 (1987).
  28. G. Franceschetti, V. Pascazio, and G. Schirinzi, "Iterative homomorphic technique for speckle reduction in synthetic-aperture radar imaging," *J. Opt. Soc. Am. A* **12**, 686–694 (1995).
  29. P. Moulin, "A wavelet regularization method for diffuse radar-target imaging and speckle-noise reduction," *J. Math. Imaging Vis.* **3**, 123–134 (1993).
  30. D. T. Kuan, A. A. Sawchuk, T. C. Strand, and P. Chavel, "Adaptive noise smoothing for images with signal-dependent noise," *IEEE Trans. Pattern. Anal. Mach. Intell.* **7**, 165–177 (1985).
  31. A. J. Healey, S. Leeman, and F. Forsberg, "Turning off speckle," *Acoust. Imaging* **19**, 433–437 (1992).
  32. J. A. Högbom, "Aperture synthesis with non-regular distribution of interferometer baselines," *Astron. Astrophys., Suppl. Ser.* **15**, 417–426 (1974).
  33. J. M. Schmitt, "Restoration of optical coherence images of living tissue using the CLEAN algorithm," *J. Biomed. Opt.* **3**, 66–75 (1998).
  34. M. D. Kulkarni, C. W. Thomas, and J. A. Izatt, "Image enhancement in optical coherence tomography using deconvolution," *Electron. Lett.* **33**, 1365–1367 (1997).